Available online at www.sciencedirect.com
ScienceDirect
Trans. Nonferrous Met. Soc. China 31(2021) 3831−3846
Transactions of Nonferrous Metals Society of China
www.tnmsc.cn

Deciphering anomalous Ag enrichment recorded by galena in Dayingezhuang Au(-Ag) deposit, Jiaodong Peninsula, Eastern China

Zhan-kun LIU[1,2], Xian-cheng MAO[1], Fan-yun WANG[3], Lei TANG[4], Guang-huan CHEN[1], Jin CHEN[1], Hao DENG[1]

1. Key Laboratory of Metallogenic Prediction of Nonferrous Metals and Geological Environment Monitoring (Ministry of Education), School of Geosciences and Info-Physics, Central South University, Changsha 410083, China;
2. Department of Geology, Lakehead University, Thunder Bay, Ontario P7B 5E1, Canada;
3. Central South University Press, Changsha 410083, China;
4. Zhaojin Mining Industry Co., Ltd., Yantai 265400, China

Received 13 October 2020; accepted 16 July 2021

Abstract: Texture, geochemistry, and in-situ Pb isotope of galena were investigated to probe the origin of anomalous Ag enrichment in the Dayingezhuang Au(-Ag) deposit. Silver enrichment postdates the main Au mineralization and occurs in the south of the Dayingezhuang deposit. It is primarily associated with galena and the exsolution of Ag-rich sulfosalts (e.g., matildite) in distal vein-ores related to steeply dipping brittle fractures. Silver-rich galena is characterized by the least radiogenic Pb isotope signature ($^{206}Pb/^{204}Pb$ 17.195–17.258 and $^{208}Pb/^{204}Pb$ 37.706–37.793), possibly indicating a metasomatized lithospheric mantle or modified lower crustal source for Pb and Ag. Both of these mafic and ultramafic source regions have been previously suggested as Au reservoirs for other Jiaodong Au deposits, implying that the metal reservoir has only a weak control on the uneven Ag-enrichment. Since the Ag-enrichment areas are located in the footwalls of both the Dayingezhuang and Zhaoping faults, the enrichment was most likely dominated by local rotational stress during coeval movements of the two faults in a NE–SW compression and NW−SE extension regime. This work highlights the shallow-crust structural deformation responsible for controlling the flow of late ore-forming fluid resulting in local anomalous metal enrichment.

Key words: galena; lead isotope; silver; Dayingezhuang deposit; Jiaodong Peninsula

1 Introduction

Orogenic Au deposits account for a large proportion of global Au reserves and are also mined for significant quantities of Ag, Te, W, Sb, and Hg [1,2]. The ore mineralogy of most orogenic deposits is typically dominated by Au, with Au/Ag concentration ratios of 1−10 and low Cu−Pb−Zn concentrations, which make them distinct from porphyry, epithermal, and Carlin-type Au deposits that have variable degrees of Ag and/or Cu enrichment [2]. The ~120 Ma Au deposits in the Jiaodong Peninsula, eastern China contain more than 5000 t Au [3]. The nature of Au mineralization in the Jiaodong gold deposits is similar to that of most orogenic Au deposits in greenstone belts. Typical characteristics include disseminated- and vein-style ore preferentially localized in detachment faults and formed from low-salinity, CO_2-rich, and moderate temperature (200−320 °C) fluids [3−9]. However, the Jiaodong deposits have been described as atypical orogenic-type deposits [3,4,8]. This is because the late timing of gold deposition relative to the age of host rocks (Precambrian greenschist- to amphibolite-facies metamorphic rocks, 160−155 Ma Linglong or Kunyushan granite, and 130−125 Ma Guojialing granite [3,5,6,10]) is at

Corresponding author: Xian-cheng MAO, Tel: +86-13707317169, E-mail: mxc@csu.edu.cn
DOI: 10.1016/S1003-6326(21)65768-0

odds with a traditional syn-metamorphic Au mineralization [11−13]. In addition, some of the Jiaodong Au deposits are unusually Ag-rich, which contrasts with the dominant Au enrichment in typical orogenic Au deposits. But, to date, few studies have focused on the cause of the Ag enrichment.

The Dayingezhuang Au(-Ag) deposit with Au resource of ~150 t [7] and Ag resource of 397 t [10] is located in the southern part of the Zhaoping fault in the western Jiaodong Peninsula (Fig. 1). Two orebodies (namely No. 1 and No. 2) separated by the east-striking Dayingezhuang fault are recognized in the deposit. The Au mineralization at Dayingezhuang is similar to other Jiaodong Au deposits but the southern segment (i.e., No. 1 orebody) is characterized by an anomalous Ag enrichment [5,10,15]. The uneven spatial distribution of Ag provides an excellent opportunity to evaluate the geological processes controlling Ag enrichment in the Jiaodong Au deposits. Previous studies have proposed multiple mechanisms to explain the anomalous Ag enrichment in the Dayingezhuang deposits, including zone refining during the main Au event, and overprinting by an Ag-rich metallogenic event that was unrelated to Au veins [5,10,15,16]. Regardless of the mechanism, the Ag source for the Dayingezhuang deposit remains unclear.

Addressing these questions requires a broad understanding of the origin of the Ag-rich fluid and its temporal and spatial evolution. Electrum and Ag-rich sulfosalts with high Ag contents can be used to investigate the Ag mineralization, but all of these phases are relatively rare in the Dayingezhuang district. Galena (PbS) with cubic crystal structure is of particular economic interest due to its close association with Ag in many types of mineral deposits, including epithermal, sedimentary-hosted, and orogenic [17−21]. It typically contains variable amounts of Ag and is also commonly intergrown with Ag-rich minerals (i.e., electrum and Ag-rich sulfosalts) in the Dayingezhuang deposit [5,10,22]. The comparable geochemical behavior of Pb and Ag in hydrothermal fluids (transported as Pb^{2+} and Ag^{+} complexes with Cl^{-} [23]) means that Pb can be used as an isotopic proxy for studying the origin of Ag.

Here, we present a comprehensive study of galena texture, geochemistry, and in-situ Pb isotopes in the Dayingezhuang Au(-Ag) deposit to

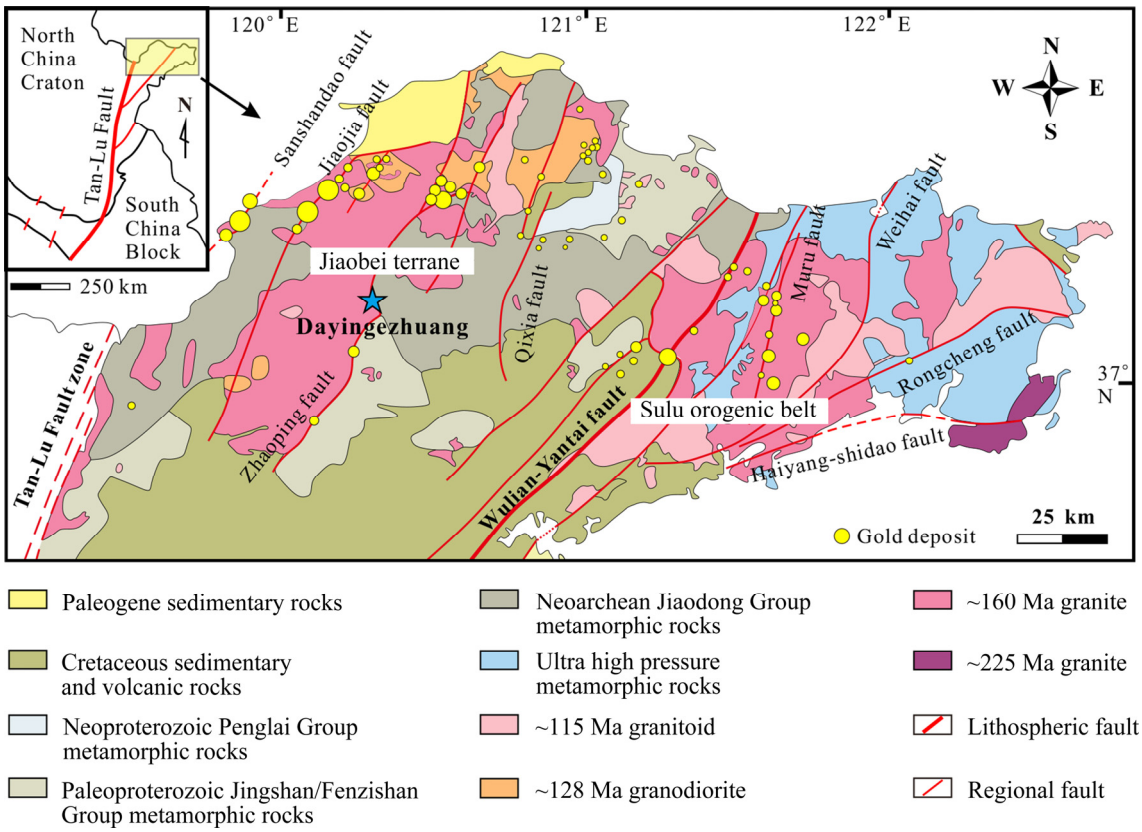

Fig. 1 Geological and tectonic map of Jiaodong Peninsula (Modified from Ref. [14])

gain a better understanding of the Pb and Ag sources and ore-forming evolution, which in turn has important genetic implications for the Dayingezhuang deposit and other Jiaodong-type orogenic Au deposits.

2 Geological background

The Jiaodong Peninsula comprises the Jiaobei terrane and the Sulu orogenic belt, which meet at the Wulian−Yantai fault (Fig. 1) [3]. More than 90% of the Au resources in the Jiaodong Peninsula are hosted by NE-striking detachment faults (e.g., Sanshandao, Jiaojia, and Zhaoping faults) in the Jiaobei terrane. The main lithologies of the Jiaobei terrane consist of Precambrian metamorphic rocks, including the Archean Jiaodong Group (tonalite−trondhjemite−granodiorite (TTG) and amphibolites), Paleoproterozoic Jingshan/Fenzishan Group metasedimentary rocks, Neoproterozoic Penglai Group metasedimentary rocks, and Mesozoic felsic intrusions (e.g., the Jurassic Linglong and Luanjiahe granite, the middle Cretaceous Guojialing granodiorite, and the late Cretaceous Aishan granite, see Fig. 1). The Linglong granite and Jiaodong Group metamorphic rocks are recognized as the primary host rocks for most of the Jiaodong Au deposits [3,4,6]. It is generally accepted that the orogenic Au deposits in the Jiaodong Peninsula formed in a narrow age range of (120±5) Ma during a tectonic transition from a compressional to an extensional setting [3,8].

The Dayingezhuang Au deposit is located in the southern portion of the Zhaoping fault in the western Jiaodong Peninsula, and is hosted by metamorphosed Archean Jiaodong Group in the hanging wall and Jurassic Linglong granite in the footwall (Fig. 2). The Jiaodong Group in the Dayingezhuang district is mainly composed of amphibolites and granulites. The Linglong granite intruded the Late Archean and Paleoproterozoic rocks and comprises plagioclase (40−50 vol.%), K-feldspar (20−25 vol.%), quartz (25−30 vol.%), and biotite (5−10 vol.%), with minor amounts of zircon, apatite, titanite, and magnetite.

The Zhaoping fault in the study area occurs along the interface between the Linglong granite and Jiaodong Group rocks (Figs. 2 and 3(a)). It generally strikes NE with dips of SE 35°−60° and shows a gentle undulation both along the strike and

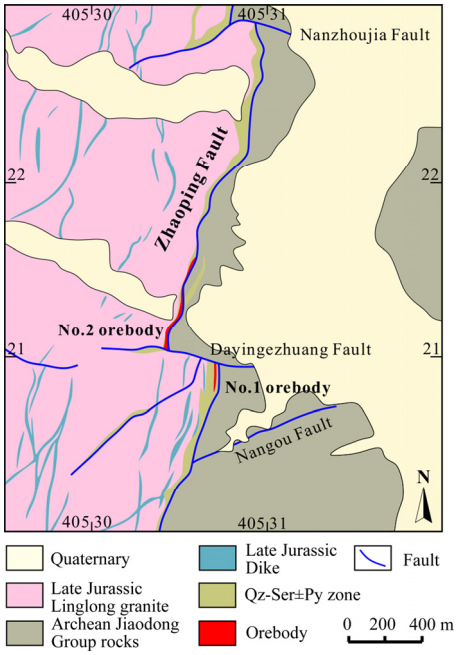

Fig. 2 Geologic map of the Dayingezhuang Au deposit in the Jiaodong Peninsula (Modified from Ref. [7])

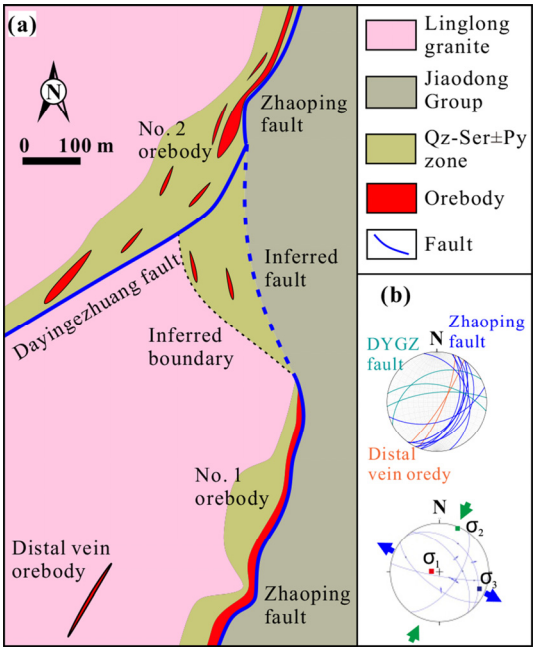

Fig. 3 Geological map at −496 m level in the Dayingezhuang Au deposit (Modified from Ref. [16]) (a), and stereonet (upper) for Zhaoping fault, Dayingezhuang fault, and distal veins (b) (The lower stereonet was generated based on measurements for ore-bearing conjugate joints and the occurrence of the Zhaoping fault, showing a NE–SW compression and NW–SE extension during ore-forming stages (σ_1 268°/77°, σ_2 23°/6°, σ_3 114°/12°). Stereonets are equal area and lower hemisphere)

dip (Figs. 3 and 4). The fault zones consist of mylonitic−ultramylonitic rocks and irregular breccias, displaying both ductile and brittle hybrid deformation characteristics [24,25]. The deformation properties change from ductile−brittle to brittle with increasing distance from the fault. The Zhaoping fault underwent at least three periods of deformation in the Jiaodong Peninsula, including sinistral torsional compression, dextral transtension and extension, and NW−SE extension [16,26]. Coeval with mineralization, the Zhaoping fault at Dayingezhuang moved in a dextral strike-slip normal sense within a NE–SW compressional and NW−SE extensional regime (Fig. 3(b)).

Several secondary faults (e.g., Nanzhoujia, Dayingezhuang, and Nangou) are present in the Dayingezhuang district (Fig. 2), of which the east striking and north-dipping (46°−59°) Dayingezhuang sinistral-slip fault with weakly normal sense has offset the Zhaoping fault (Figs. 4(a, b)). The Dayingezhuang fault is only found at depths less than 700 m. There is a transition of dip direction from north-dipping at the surface to NW-dipping at depth (Figs. 2 and 3(a)). Minor quartz−sericite−pyrite alteration and gold orebodies are spatially associated with the Dayingezhuang fault (Figs. 2 and 3(a)).

Major Au mineralization in the Dayingezhuang deposit is developed in the footwall mylonization and brecciation zone proximal to the Zhaoping fault associated with brittle−ductile deformation (Fig. 5). It comprises two orebodies (No. 1 and No. 2 in Figs. 2 and 4(c)). The No. 2 orebody in the north segment accounts for about 65% of Au

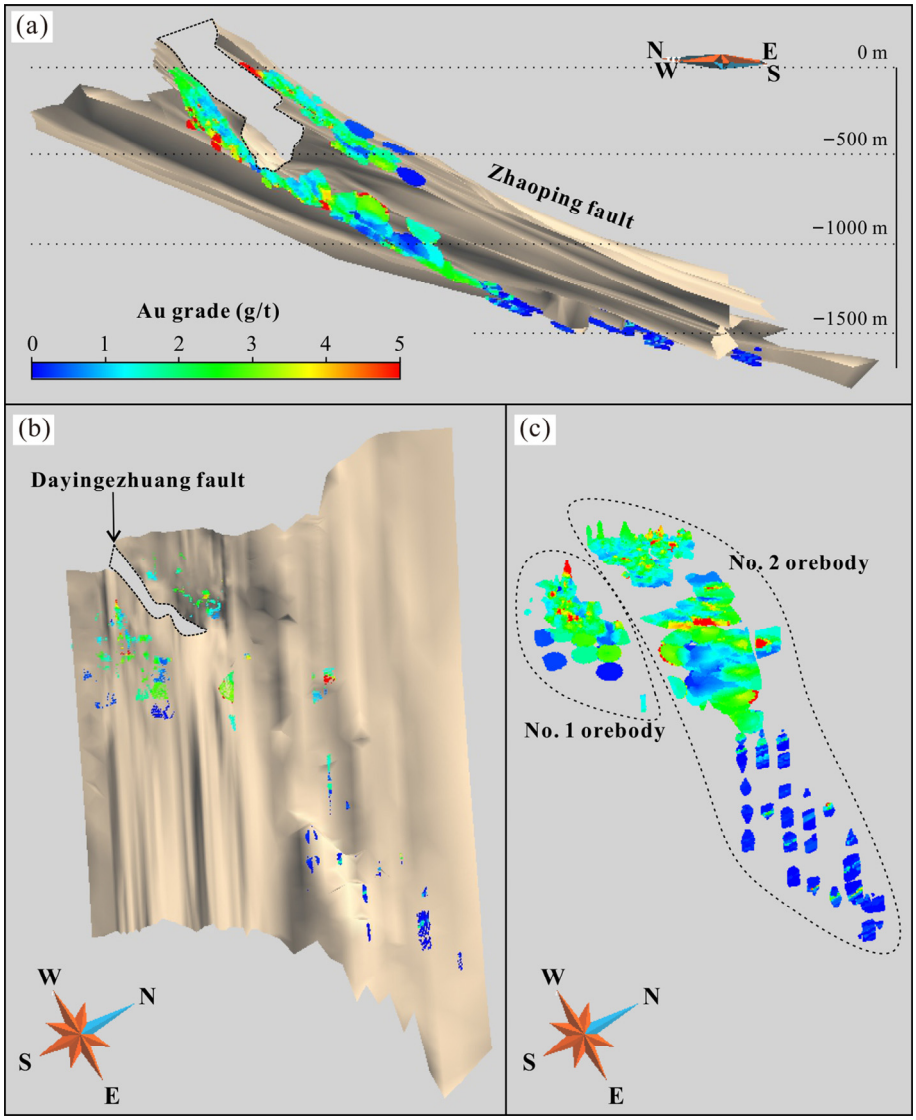

Fig. 4 3D models showing Zhaoping fault (a), Dayingezhuang fault (b), orebodies (c), and Au distribution (The cut off grade for economic orebodies is 1 g/t. More information about the models is provided in Ref. [7])

resources and consists of disseminated mineralization associated with quartz−sericite−pyrite alteration and intense deformation (Figs. 6(a, b)). It extends along strike for more than 3000 and 1500 m down-dip (NE), with Au grades typically <5 g/t (Fig. 4(c)). The No. 1 orebody is located in the southern portion of the Dayingezhuang deposit, which is about 1500 m in length, and has

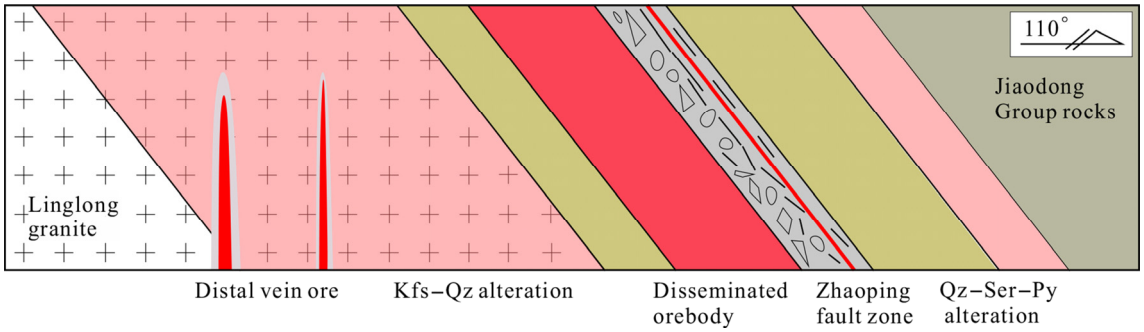

Fig. 5 Schematic diagram illustrating general spatial relationships of mineralization, alteration, fault, and wall rocks in the Dayingezhuang deposit (Kfs−K-feldspar; Py−Pyrite; Qz−Quartz; Ser–Sericite)

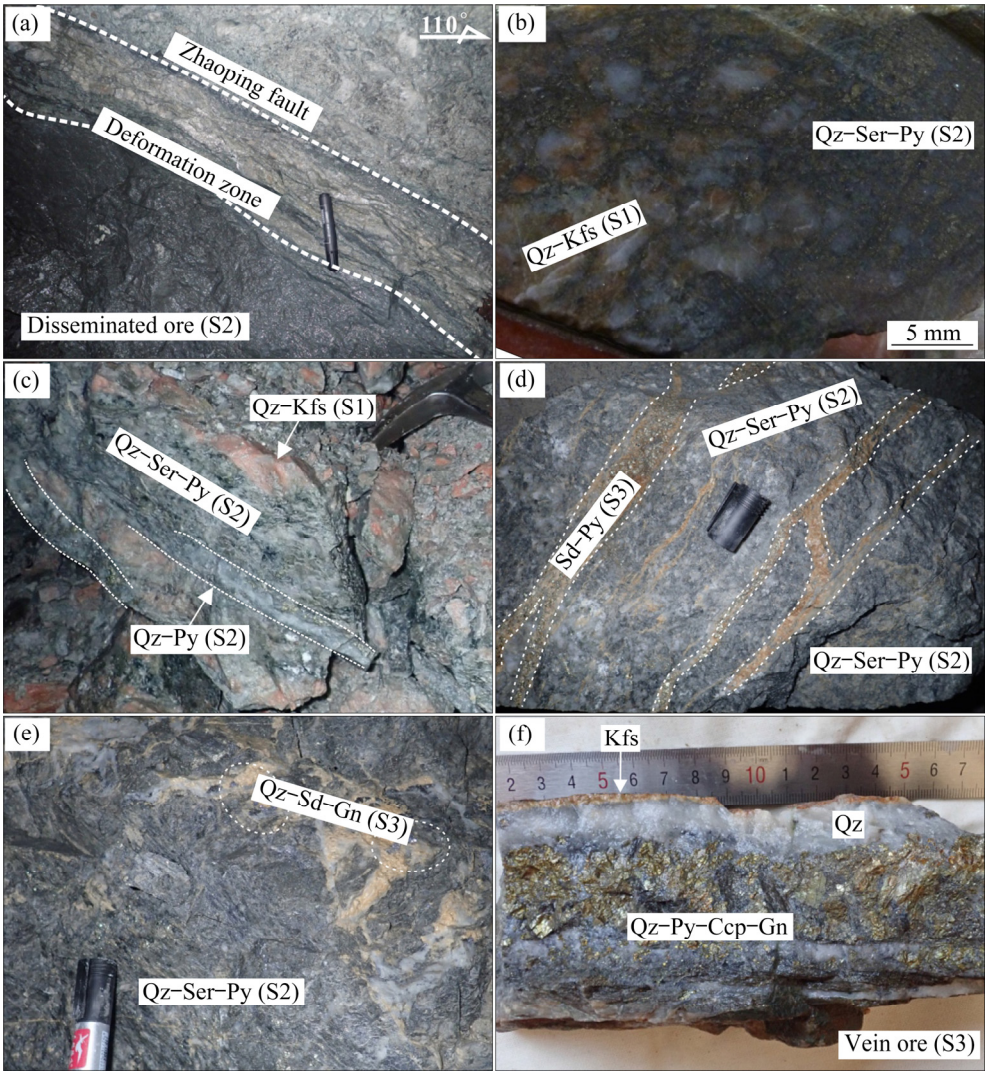

Fig. 6 Photos of alteration and mineralization in the Dayingezhuang deposit: (a) Disseminated ore in footwall of the Zhaoping fault; (b) Quartz−sericite−pyrite alteration replacing early quartz−K-feldspar alteration; (c) Quartz−sericite−pyrite altered rocks that cement early quartz−K-feldspar fragments crosscut by quartz−pyrite vein; (d, e) Early quartz−sericite−pyrite alteration crosscut by late siderite-pyrite or quartz−siderite−galena vein; (f) Quartz−polymetallic sulfide vein from distal vein orebody with anomalous high Au(-Ag) grades (Gn–Galena, Sd–Siderite)

Au grades ranging from 2 to 4 g/t. Two mineralization styles are present within the No. 1 orebody: (1) gently-dipping disseminated ore proximal to the Zhaoping fault; (2) steeply-dipping vein ore distal to the Zhaoping fault (Figs. 3(a) and 5). The vein-style mineralization occurs as fill in extensional and steeply dipping brittle fractures and typically shows vein or veinlet features in the weakly potassic or fresh Linglong granite. Overall, the No. 2 orebody shows more complex geometric features than the No. 1 orebody: the former is marked by the pinch-and-swell geometries whereas the latter undulates gently parallel to the Zhaoping fault [15,16,27]. Silver is markedly enriched in the No. 1 orebody, especially in the distal vein ore. The Ag grade (average 15 g/t) gradually increases from shallow to deep levels in the No. 1 orebody [5]. Silver mineralization always accompanies the Au mineralization in the Dayingezhuang deposit. The available geochronology data reveal that the No. 1 orebody postdates the No. 2 orebody (119−127 Ma vs. 133−128 Ma) [5,10].

The major Au(-Ag) mineralization in the Dayingezhuang deposit is closely associated with quartz−sericite−pyrite alteration (Figs. 6(a−e)) and quartz−polymetallic sulfide veins (Figs. 6(c−f)). Gold is mainly hosted in electrum (Figs. 7(d−f)) and Ag-bearing native gold that occurs as free grains or filling associated with quartz and/or sulfide with minor amounts as inclusions within sulfide. Silver occurs as a component of the Au−Ag mineral series and also in galena, argentite (Ag_2S), $PbAgBiS_3$ (Figs. 7(g, h)), matildite ($AgBiS_2$; Fig. 7(i)), stromeyerite (AgCuS), and freibergite ($(Cu,Ag)_6Cu_4Sb_4S_{13}$) [10]. These Ag-bearing minerals are generally associated with galena in the

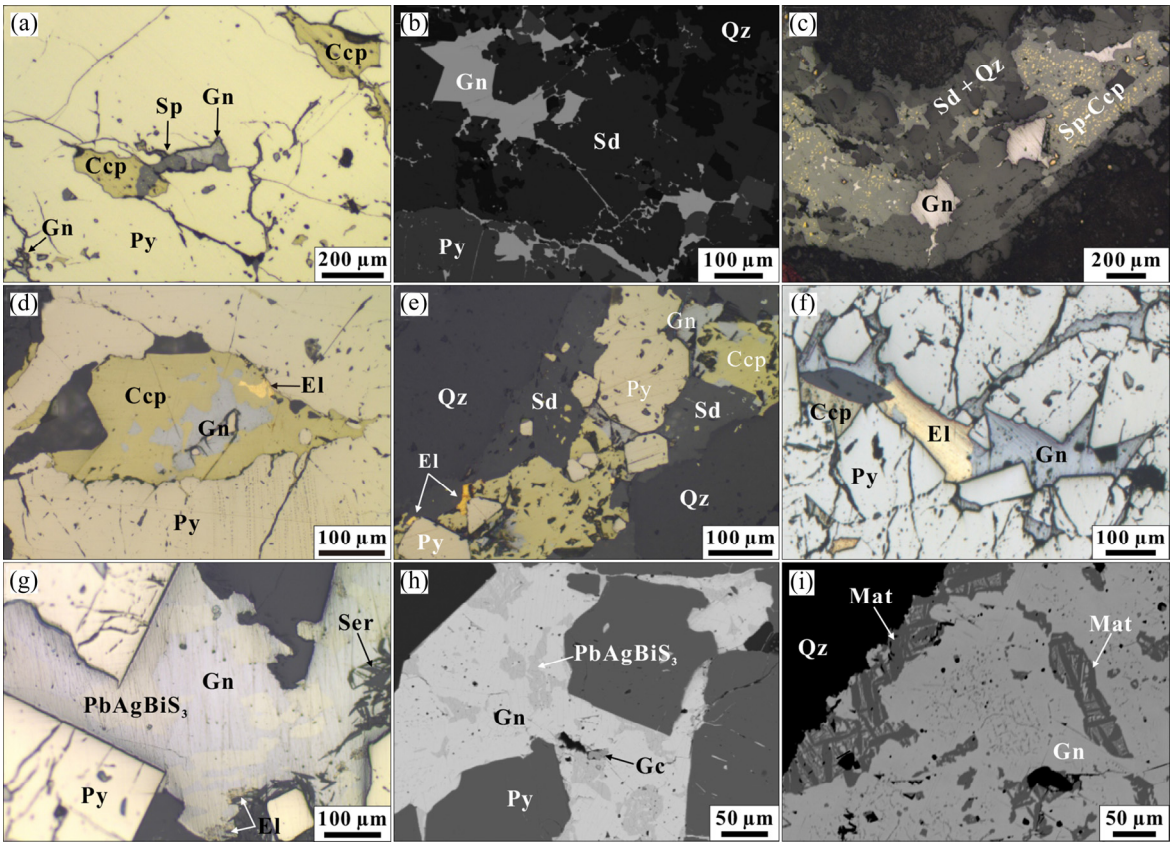

Fig. 7 Reflected-light photos (a, c–g) and BSE images (b, h, i) of galena in the Dayingezhuang deposit: (a) Galena intergrown with sphalerite and chalcopyrite, No. 2 orebody; (b) Anhedral galena hosted in fractures of siderite and pyrite, No. 2 orebody; (c) Polymetallic sulfide–siderite–quartz vein, No. 1 orebody, sphalerite with chalcopyrite exsolution texture; (d) Intergrowth of chalcopyrite, galena, and electrum in coarse-grained pyrite, No. 1 orebody; (e) Typical auriferous polymetallic sulfide–siderite vein, No. 1 orebody; (f) Electrum, galena, and chalcopyrite filling open fractures in pyrite, No. 1 orebody; (g, h) Coarse-grained galena with $PbAgBiS_3$ exsolution texture, distal vein ore of No. 1 orebody; (i) Lamellae matildite within galena showing Widmanstätten-like textures (i.e., solid exsolution), distal vein ore of No. 1 orebody (Ccp–Chalcopyrite, El–Electrum, Gc–Greenockite, Mat–Matildite, Sp–Sphalerite)

quartz−polymetallic sulfide−siderite veins.

Based on the mineral assemblages and crosscutting and overprinting relationships, four paragenetic sequences have been identified in the Dayingezhuang deposit (Fig. 8 [10,28]). Stage 1 (S1), the pre-ore stage, is characterized by the assemblage of K-feldspar, quartz, pyrite, and sericite (Figs. 6(b, c)). Stage 2 (S2), the major Au mineralization stage, is marked by intense quartz−sericite−pyrite alteration coupled with strong brecciation (Figs. 6(a−e)). Major minerals of Stage 2 include quartz, sericite, pyrite, and minor siderite, chalcopyrite, and electrum. Stage 3 (S3) comprises Au and Ag mineralization and precipitation of quartz, siderite, polymetallic sulfide (e.g., galena, chalcopyrite, and sphalerite), and minor electrum and sulfosalts (Fig. 7). The polymetallic sulfide occurs in irregular aggregates filling cavities or cracks within pyrite (Figs. 7(a−d, f)) or as intergrowths with quartz and siderite in quartz−carbonate polymetallic veins (Figs. 7(b, c, e)). The Stage 3 minerals typically comprise veins, stockworks, and veinlets crosscutting previous quartz−sericite−pyrite or K-feldspar altered rocks (Figs. 6(d, e)). Stage 4 is the post-ore stage and is marked by white calcite veins [10,28].

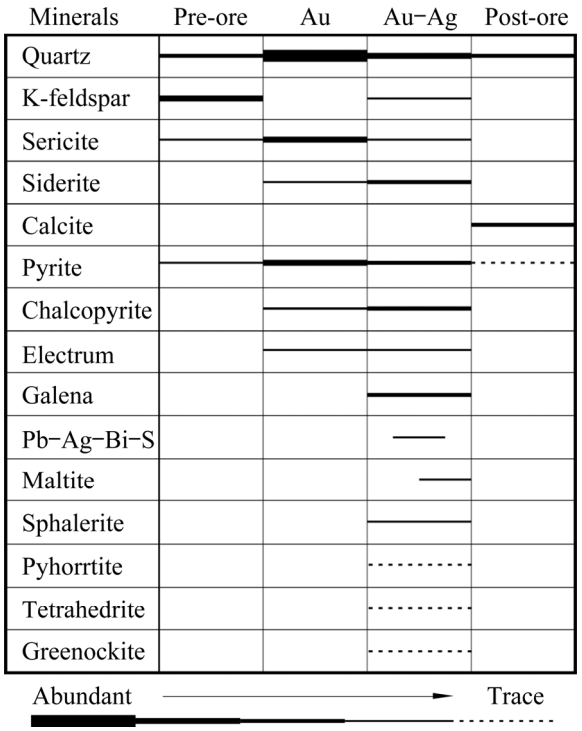

Fig. 8 Paragenetic mineral sequence for the Dayingezhuang gold deposit

3 Analytical methods

Geochemical analysis of galena was performed at the Wuhan Microbeam Analysis Technology Co., Ltd., China, using a JEOL JXA−8230 Electron Probe Microanalyzer (EPMA) equipped with five wavelength-dispersive spectrometers (WDS) [29]. Operating conditions for quantitative WDS analyses involved an accelerating voltage of 20 kV, a beam current of 20 nA, and a 1 μm spot size. The X-ray peak and background intensities were measured for 10 and 5 s, respectively. The following standards were used: galena (S, Pb), bismuth (Bi), silver (Ag), tin (Sn), stibnite (Sb), cadmium (Cd), tellurium (Te), pyrite (Fe), chromium (Cr), and copper (Cu). Data were corrected using a JEOL oxide-ZAF (atomic number, absorption and fluorescence) correction procedure. Tin, Sb, and Cu are mostly below detection limits and are not reported in this work.

In-situ Pb isotope analyses of galena were conducted with a Neptune Plus MC-ICP-MS equipped with a Geolas HD excimer ArF laser ablation system at the Wuhan Sample Solution Analytical Technology Co., Ltd., China. Galena was ablated using a spot diameter of 10 μm with a pulse frequency of 2 Hz and a laser fluency of ~6 J/cm^2. Isotopes ^{208}Pb, ^{207}Pb, ^{206}Pb, ^{204}Pb, ^{205}Tl, ^{203}Tl, and ^{202}Hg were collected in Faraday cups using the static mode. The mass discrimination factor for Pb was determined using a Tl solution of NIST SRM 997 nebulized at the same time as the sample, using an Aridus II desolvating nebulizer. The mass fractionation of Pb isotopes was corrected by ^{205}Tl/^{203}Tl using the exponential law. Two Pb isotope standards MASS-1 and Sph-HYLM were used to obtain the optimized values of ^{205}Tl/^{203}Tl to correct for mass fractionation of Pb and Tl. The ^{202}Hg signal was obtained to correct the remaining ^{204}Hg interference on ^{204}Pb, using the natural ^{202}Hg/^{204}Hg ratio of 0.2301. The accuracy is better than ±0.2‰ for ^{208}Pb/^{204}Pb, ^{207}Pb/^{204}Pb, and ^{206}Pb/^{204}Pb ratios.

4 Results

The galena geochemistry and Pb isotope data are provided in Table 1. The Pb and S concentrations of galena from the No. 2 and No. 1 disseminated orebodies vary in the similar range

Table 1 Geochemical compositions and Pb isotope ratios of galena from the Dayingezhuang deposit

No.	Composition/wt.%								Isotope ratio		
	Pb	S	Bi	Ag	Cd	Te	Fe	Cr	$^{206}Pb/^{204}Pb$	$^{207}Pb/^{204}Pb$	$^{208}Pb/^{204}Pb$
19-1*	83.82	13.32	0.77	0.09	0.14	0.06	0.01	0.86	17.305	15.478	37.885
19-2*	84.42	13.34	0.77	0.12	0.10	0.04	0.04	0.75	17.307	15.476	37.872
19-3*	85.69	13.52	0.77	0.11	0.12	–	0.03	0.96	17.290	15.473	37.871
19-4*	84.21	13.27	0.75	0.07	0.12	–	0.03	–	17.293	15.463	37.833
19-5*	85.25	13.43	0.62	0.02	0.11	–	0.30	0.74	17.294	15.473	37.889
19-6*	84.83	13.62	0.86	0.19	0.13	–	0.09	–	17.296	15.469	37.868
54-1*	84.44	13.38	1.57	0.46	0.07	0.03	0.05	–	17.299	15.472	37.860
54-2*	84.38	13.38	1.60	0.47	0.07	0.04	0.05	0.00	17.301	15.469	37.866
56-1*	84.93	13.26	1.02	0.20	0.12	–	0.05	–	17.304	15.478	37.885
56-2*	83.41	13.34	1.50	0.40	0.11	–	0.06	–	17.302	15.475	37.859
105-1#	84.11	13.55	1.42	0.48	0.09	–	0.12	–	17.229	15.462	37.829
105-2#	82.90	13.47	1.81	0.60	0.10	–	0.04	–	17.236	15.469	37.838
108-1#	85.11	13.17	0.46	–	0.09	0.00	0.02	–	17.268	15.466	37.833
108-2#	85.10	13.19	0.41	–	0.13	0.05	0.02	–	17.281	15.475	37.863
108-3#	85.44	13.35	0.43	–	0.12	–	0.01	1.27	17.264	15.463	37.834
108-4#	85.23	13.21	0.47	–	0.10	0.05	0.01	–	17.272	15.469	37.823
14-1#	84.00	13.13	0.71	0.05	0.14	0.04	0.02	1.17	17.252	15.469	37.838
14-2#	82.97	13.52	2.30	0.79	0.08	0.03	0.06	–	17.250	15.471	37.848
66A-1^	73.96	13.94	7.48	3.35	0.12	0.00	0.02	–	17.221	15.453	37.793
66A-2^	80.34	13.88	4.19	1.71	0.11	–	0.05	0.33	17.258	15.469	37.786
66B-1^	76.53	13.73	5.56	2.62	0.13	0.07	0.09	–	17.195	15.434	37.706
66B-2^	78.33	13.60	4.58	2.13	0.07	–	0.10	–	17.211	15.446	37.762
66B-3^	79.23	13.61	4.89	2.31	0.11	0.04	0.05	–	17.221	15.461	37.766
66B-4^	78.03	13.42	4.42	1.99	0.09	0.11	–	–	17.207	15.450	37.764
67-1^	77.44	13.58	4.77	2.23	0.09	0.02	0.07	–	17.222	15.450	37.769
67-2^	78.03	13.30	4.64	2.01	0.10	0.05	0.17	–	17.214	15.452	37.768
112-1^	80.01	13.54	3.74	1.50	0.07	0.04	0.13	2.26	17.220	15.463	37.786
112-2^	84.82	13.35	1.18	0.28	0.11	0.03	0.05	–	17.210	15.460	37.761

Note: Markers * denote that samples are collected from No. 2 disseminated ore, # samples from No. 1 disseminated ore, and ^ from No. 1 vein ore. "–" is below detection limit

of 82.90−85.69 wt.% and 13.13−13.62 wt.%, respectively, whereas the galena in veins from the No. 1 orebody has lower Pb contents (mostly <80 wt.%). Silver is particularly enriched in the galena hosted in the veins (average 2.01 wt.%, Table 1). All galena samples at Dayingezhuang are distributed along the galena−matildite trend (Fig. 9(a)). Trace concentrations of Bi and Ag are positively correlated (R^2>0.98, Fig. 9(b)). Measured Pb concentrations negatively correlate with Bi and Ag in most galena samples (Table 1, Fig. 9(c)).

The results for galena from several orebodies in the Dayingezhuang deposit exhibit different clusters in conventional $^{206}Pb/^{204}Pb$ vs. $^{207}Pb/^{204}Pb$ and $^{206}Pb/^{204}Pb$ vs. $^{208}Pb/^{204}Pb$ diagrams (Fig. 10). Galena intergrown with Ag-bearing sulfosalt minerals in the distal vein ore yields the least radiogenic Pb isotope ratios ($^{206}Pb/^{204}Pb$=17.195−17.258, $^{207}Pb/^{204}Pb$=15.434−15.469, and $^{208}Pb/^{204}Pb$ =37.706−37.793), whereas galena from the major

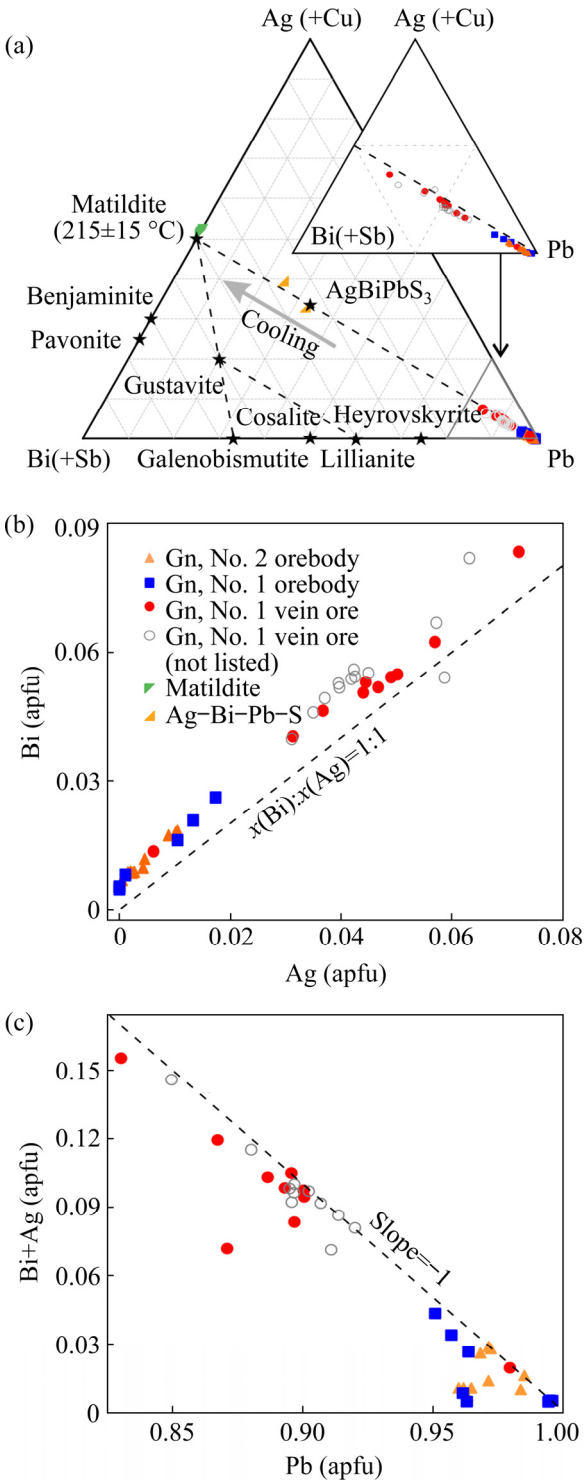

Fig. 9 Ag(+Cu)–Bi(+Sb)–Pb ternary diagram (a) of Ag–Bi–Pb–S sulfosalt minerals illustrating galena–matildite solid solution in the Dayingezhuang deposit, binary plots of Ag and Bi (b), and binary plots of Pb and Bi+Ag (c) (Data for matildite (n=5), Ag–Bi–Pb–S minerals (n=2), and some galena samples (n=12) from vein ore are taken from our unpublished data. Before plotting data were normalized to Σ2 atoms. apfu is atoms per formula unit)

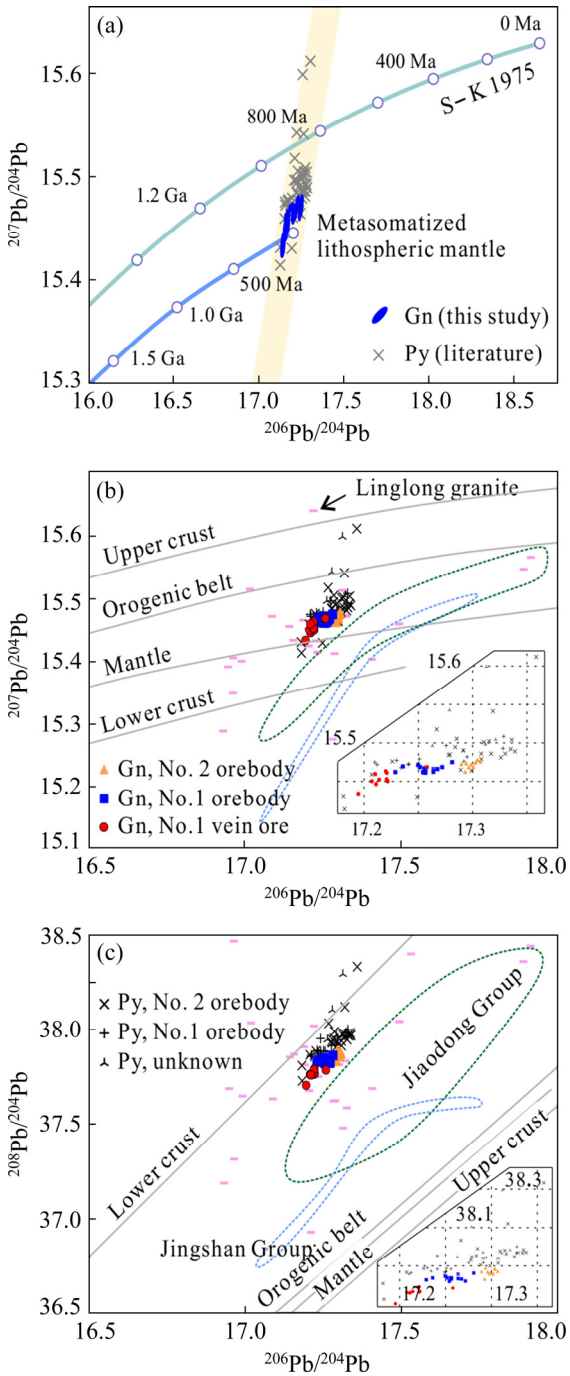

Fig. 10 Evolution of unradiogenic Pb isotopes of pyrite and galena from the Dayingezhuang deposit (a) (The two-stage crust growth curve (S−K 1975) is from Ref. [30], and the metasomatized lithospheric mantle curve involves a combination of Archean juvenile crust and/or previously melt-depleted and subsequently metasomatized lithospheric mantle. More details about the parameters are provided in Ref. [31]) and $^{206}Pb/^{204}Pb$ vs. $^{207}Pb/^{204}Pb$ (b) and $^{206}Pb/^{204}Pb$ vs. $^{208}Pb/^{204}Pb$ (c) diagrams [32] comparing sulfide Pb isotope signature of the Dayingezhuang deposit with regional lithologies and previously published global Pb evolution models

No. 1 orebody proximal to the Zhaoping fault yields slightly high Pb isotope ratios ($^{206}Pb/^{204}Pb$= 17.229−17.281, $^{207}Pb/^{204}Pb$=15.461−15.475, and $^{208}Pb/^{204}Pb$=37.821−37.863). Isotope results from the No. 2 orebody trend to more radiogenic signatures ($^{206}Pb/^{204}Pb$=17.290−17.307, $^{207}Pb/^{204}Pb$ =15.463−15.478, and $^{208}Pb/^{204}Pb$=37.889−38.833) relative to those of the No. 1 orebody. The new galena results for galena in this study overall yield less radiogenic compositions than previously published Pb isotope data for pyrite (Fig. 10).

The geochemistry and Pb isotope systematics are further investigated using principal component analysis (PCA) and represented as a PCs biplot in Fig. 11. The first principal component (PC1) plus second principal component (PC2) account for 65.4% of the dataset variance. Multivariate analysis highlights three groups of galena analyses from the Dayingezhuang deposit (Fig. 11). Most galena samples from No. 2 and No. 1 major orebodies yield positive PC1 (0, 3) and variable PC2 (−2, 1.5). These analyses tend to be associated with the high Cr and Pb concentrations and high $^{206}Pb/^{204}Pb$, $^{207}Pb/^{204}Pb$, and $^{208}Pb/^{204}Pb$ ratios. Galena from vein ore yields negative PC1 scores, corresponding to high Bi, Ag, S and low Pb contents and low Pb isotopic ratios.

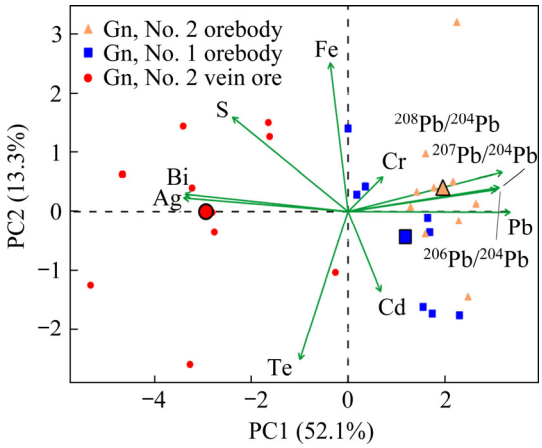

Fig. 11 Principal component analysis (PCA) of major elements and Pb isotope data for galena at the Dayingezhuang deposit (The three large symbols denote the center points of three groups of galena. The PCA was completed following the procedure of Ref. [33])

5 Discussion

5.1 Element substitution in galena

Galena with cubic structure (*Fm3m*) is of particular economic interest due to its incorporation of Ag as an original component into its crystal structure [19]. Previous studies have shown that the Ag substitution mechanism likely involves at least two exchange vector reactions: (1) $2Ag^{+} \leftrightarrow Pb^{2+}$, and (2) $Ag^{+} + (Sb, Bi)^{3+} \leftrightarrow 2Pb^{2+}$ or $(Ag, Tl, Cu)^{+} + (Sb, Bi)^{3+} \leftrightarrow 2Pb^{2+}$ [19,20,34,35]. The former is expected to contribute minor to moderate amounts of Ag (<0.37 wt.%) owing to unfavorable energetics and its location in octahedral sites, whereas the latter substitution reaction can significantly impact Ag uptake (up to 9 wt.%) [34,35]. Some previous studies also report Ag^{0} in galena associated with low S, Sb, and Bi activities and high Ag activity in hydrothermal solutions [20]. Nevertheless, the Ag^{0} occurs in very low amounts. Galena from the Dayingezhuang deposit commonly contains variable amounts of Bi that positively correlate with the Ag contents of 0−3.35 wt.% (Figs. 9(b) and 11). The Ag−Bi element association, coupled with the extremely low concentrations of Sb and Cu (all below detection limit), suggests that Ag enrichment within the Dayingezhuang galena is primarily controlled by a coupled substitution of $Ag^{+}+Bi^{3+} \leftrightarrow 2Pb^{2+}$. However, nearly all galena samples plot above the $x(Ag)/x(Bi)$=1:1 line (Fig. 9(b)), reflecting an excess Bi (about 0.007 apfu). The possible mechanisms may include solid solution through $2Bi^{3+}$ + vacancy $\leftrightarrow 3Pb^{2+}$, which is likely to occur when Bi is relatively abundant in the hydrothermal fluids responsible for precipitating galena [19]. Given the $PbAgBiS_3$ and matildite exsolution from galena, the ore-forming fluids were likely enriched in Bi, consistent with the element substitution mechanism $2Bi^{3+}$ + vacancy $\leftrightarrow 3Pb^{2+}$ in galena. Both of the proposed substitution mechanisms are also consistent with multivariate analyses, demonstrating that Bi and Ag are positively correlated and yield high loadings along PC1. Besides, tellurium, as the only element with both negative PC1 and PC2 scores, is to some extent positively correlated with Bi and Ag, and negatively with Pb (Fig. 11), perhaps indicating a charge balance for the substitution of Pb by Bi and Ag in galena. The significant co-variations between Te and Bi and Ag were also documented in previous studies [19]. In conclusion, trace metals such as Ag and Bi were likely incorporated into galena at Dayingezhuang by a combination of substitution reactions in Pb sites.

5.2 Metal sources

The Ag(-Au) mineralization in the Dayingezhuang deposit is closely associated with galena and its coexisting electrum and Ag-bearing sulfosalts (e.g., $PbAgBiS_3$ and matildite; Figs. 7(g–i)). The $PbAgBiS_3$−galena and lath-like matildite−galena intergrowths as well as the partitioning of Ag−Bi−Pb in galena (Fig. 9(a)) are consistent with the Ag−Bi−Pb−S solid solution series in the Dayingezhuang deposit. The observation probably reflects the exsolution process associated with cooling (to (215±15) °C) of an initial high-temperature (likely >400 °C) homogeneous phase [17,18,35−37]. If correct, this means that Pb and Ag were homogeneous in deep (>10 km) high-temperature hydrothermal fluids before ascending into the shallow (5−10 km [3]) mineral system. Such a fluid condition is conducive to the transport of metals and complexes from the source region to shallow trap areas in a mineral system [38]. Due to the high Ag contents (average 2.01 wt.%) of galena in the distal vein ore (Table 1), we propose that a deep-seated (>10 km) Ag- and Pb-rich hydrothermal fluid was likely involved in the high-grade Ag(-Au) mineralization during Stage 3.

Galena rarely incorporates U during the crystallization and thus its measured lead isotope data directly represent the initial isotopic composition when it precipitated [33]. The galena Pb isotope data from this study show typically less radiogenic Pb than previously published pyrite results (Fig. 10), which plot close to the two-stage evolution curve (S−K 1975 in Fig. 10(a)) [30] that represents a general continental crust growth. Less radiogenic galena signatures tend to be associated with the highest concentrations of Ag and Bi in multivariate space (Fig. 11). Such characteristics suggest that trace concentrations of Pb within pyrite were likely derived from more radiogenic upper crust and/or contain a small but variable proportion of radiogenic Pb from in situ decay, and Pb and Ag were closely associated with primitive and relatively unradiogenic Pb reservoirs. The pyrite in the Dayingezhuang Au deposits is commonly depleted in most trace elements, and its Pb concentrations are highly variable ($<1\times10^{-6}$ to 10^{-3}; mostly below 20×10^{-6}) due to the occurrence of Pb-bearing mineral inclusions, such as galena and/or silicate inclusions [22]. The more radiogenic Pb in pyrite is likely the result of inclusions of Pb-bearing silicate inclusions (e.g., feldspar) since the host Linglong granite is more radiogenic than all other lithologies at Dayingezhuang (Figs. 10(b, c)). In contrast to the pyrite, Pb is a major element in galena and is rarely affected by mineral inclusions as suggested by the homogeneous laser profiles (not shown) for several Pb isotopes. The less radiogenic Pb signature of galena is perhaps more representative of the Pb (and Ag) source of the Dayingezhuang deposit, because it is less affected by radiogenic in-growth and is more closely associated with the Ag-rich mineral assemblage.

Regardless of the difference in Pb isotopes of galena and pyrite, both minerals yield low Pb isotope ratios ($^{206}Pb/^{204}Pb < 17.36$, Table 1) and considerably older model ages (>800 Ma, Fig. 10(a)) than the inferred timing of mineralization (ca. 120 Ma). This suggests an old and/or relatively unradiogenic Pb reservoir as major metal sources (e.g., older rocks in the basement, previously melt-depleted lower crust or lithosphere upper mantle) rather than the juvenile crust or subduction-related components [39−41]. New Pb isotope results are also distinct from the expected signature of melts and/or fluids at the mineralization age (~120 Ma), suggesting that at least some of the ore-forming components in the Dayingezhuang Au deposit were remobilized from an old reservoir rather than having a direct association with paleo-Pacific plate subduction during the Mesozoic. Furthermore, all of the Pb isotope data for the Dayingezhuang sulfide samples plot along a steeply sloping trend on the $^{206}Pb/^{204}Pb$ vs. $^{207}Pb/^{204}Pb$ diagram, reflecting a mixed Pb isotopic source [40,42]. Most data are below the S−K 1975 curve but above the previously melt-depleted and subsequently metasomatized lithospheric mantle (Fig. 10(a)), suggesting a mixed source of crust and/or metasomatized lithospheric mantle.

Possible source rocks within the lower to upper crust of the western Jiaodong Peninsula include the Precambrian Jiaodong and Jingshan formation and Mesozoic magmatic intrusions that were derived from melting the old lower crust [43−46]. Overall, the sulfide Pb isotope data overlap with the Linglong granite on $^{207}Pb/^{204}Pb$ and $^{208}Pb/^{204}Pb$ vs. $^{206}Pb/^{204}Pb$ plots (Figs. 10(b, c)),

suggesting broadly similar compositions. The Linglong granite is the major host rock for some of the Au deposits and commonly developed intense quartz−sericite−pyrite alteration and brecciation during mineralization (Figs. 6(a−e)). It is possible that Pb-bearing minerals (e.g., feldspar) within the host granite were dissolved and then transported by the ore-forming hydrothermal fluids. The remobilization of Pb from the shallow Linglong granite is a plausible mechanism for generating the crustal-sourced radiogenic Pb. This could also explain the galena with the least radiogenic Pb isotope ratios, especially from the vein ore, since in the Dayingezhuang deposit they commonly occur as vein fill (Figs. 6(d−f)), during which the fluid-rock interaction is weaker compared to the disseminated ores associated with the fractured quartz−sericite−pyrite altered rocks.

Metasomatized and previously melt-depleted lithospheric mantle, lower crust, and/or the Jiaodong and Jingshan Group metamorphic rocks likely contributed the less radiogenic Pb to the Dayingezhuang galena (Fig. 10). However, the vein ore of the No. 1 orebody is located in the Linglong granite in the footwall of the Zhaoping fault (Figs. 3(a) and 5), which is unlikely to represent a possible source region based on the low Pb isotope ratios of galena and the low-degree of water/rock interaction. This likely points to long distances transport of Pb–Ag(–Au)-rich fluids. Hence, the shallow and/or exposed metamorphic and igneous host rocks can be ruled out as the source of the least radiogenic Pb.

In summary, Pb and Ag of the Dayingezhuang deposit were mainly derived from the metasomatized subcontinental lithospheric mantle and/or modified lower crust, and shallow country rocks (e.g., Linglong granite) likely contributed only minor Pb into the mineral system by fluid−rock interaction.

5.3 Genetic and exploration implications

The results of this study show that the metasomatized lithospheric mantle and/or modified low crust are possible sources for Ag-rich fluids in the Dayingezhuang deposit. Due to the consistent behavior of Ag and Au in the moderate to high temperature hydrothermal solutions as the monovalent Au^+ and Ag^+ complexes with Cl^- and/or HS^- ligands [47−49], the interpretation that the Ag and Au were derived from similar reservoirs offers a likely explanation for the ubiquitous occurrence of electrum and rare occurrence of native gold in the Jiaodong Au deposits. This further implies that source controls are important for the diversity of metal enrichment in orogenic Au deposits. The timing and relatively short duration of mineralization ((120±5) Ma) that resulted in exceptional Au(-Ag) accumulation (>5000 t) in the Jiaodong Peninsula suggests that the tectonic trigger for mineralization is presumably one of the most important controlling factors. During the Late Mesozoic, craton destruction and lithospheric thinning associated with asthenospheric upwelling following the paleo-Pacific subduction may have provided sufficient energy to mobilize deep-seated fluids in the subcontinental lithospheric mantle and/or lower crust [3].

The anomalous Ag enrichment in the No. 1 orebody of the Dayingezhuang deposit is distinct from most Jiaodong Au deposits [5,7,10,15]. At Dayingezhuang, the peculiarity of Ag-rich galena from the distal vein ore is further reflected by less radiogenic Pb that is dissimilar to other ore-forming mineral phases (e.g., pyrite). These slightly low Pb isotope ratios likely reflect a higher proportion of more deeply sourced metals in the Ag-rich hydrothermal fluids. Despite the somewhat unusual Pb isotope signature of the Ag-rich galena, most galena samples are indistinguishable from other Au deposits in the Jiaodong Peninsula [3], which implies that the Ag mineralization is not uniquely controlled by the source region.

Generally, the Ag enrichment in the Dayingezhuang deposit is mainly associated with Ag-bearing sulfosalt minerals and galena in the distal S3 quartz-polymetallic sulfide veins and overprinted disseminated ore (Fig. 6). The crosscutting relationship between the polymetallic sulfide veins and quartz−sericite−pyrite altered rocks strongly suggests the Ag(-Au) enrichment in S3 happened later than primary Au mineralization. This is further supported by the available geochronology data, which indicates that the Ag-rich No. 1 orebody postdates the No. 2 orebody (119−127 Ma vs. 133−128 Ma) [5,10]. Combined with the deep-seated ore-forming fluids for the high-grade Ag(-Au) mineralization of distal veins as discussed above, the S3 Ag(-Au)-rich fluids likely represent a late individual fluid pulse after

the Au mineralization event associated with S2 quartz−sericite−pyrite alteration.

Field observations show that the S3 quartz-polymetallic sulfide vein in the No. 2 orebody is relatively limited relative to the No. 1 orebody [10]. Previously published results demonstrated that the fluids of the main ore-stage in the No. 1 orebody are characterized by inclusions with SO_4^{2-}<Cl^- and K^+<Na^+ and higher Cl^- concentrations than the fluids of the No. 2 orebody [15]. High salinity fluids tend to favor transport of Ag and Pb, because the two metals are transported by chloride-complexes in hydrothermal fluids and their concentrations correlate with salinity (i.e., NaCl contents) [50−52]. Hence, the Ag-enrichment in the No. 1 orebody may be attributed to the more overprinting of the S3 polymetallic sulfide veins than No. 2 orebody.

Although the No. 1 and No. 2 orebodies in the Dayingezhuang deposit seem to be offset by the Dayingezhuang fault (Figs. 2 and 3(a)) [5,10,27], our 3D models reveal that the two orebodies are not spatially continuous in the areas without development of the Dayingezhuang fault (Fig. 4(c)). Notably, Au mineralization is partly developed in the Dayingezhuang fault zone (Fig. 3(a)) [27]. This suggests that the Dayingezhuang fault formed prior to gold mineralization and there was movement of the fault during ore formation. With increasing depth, the Dayingezhuang fault becomes steeper and the dip direction changes from N to NW (Figs. 3(a) and 4(a, b)). Our structural investigation (Fig. 3(b)) shows that the Zhaoping fault in the Dayingezhuang district has moved in a dextral strike-slip normal sense in a transtension-extension environment (σ_1 nearly vertical and σ_3 NEE–SWW). The fault movement likely accompanied local torsion was conducive to generating the changes of dip direction and angle of the Dayingezhuang fault. Since the south segment of the Dayingezhuang deposit is located in the footwalls of both the Dayingezhuang and Zhaoping faults, the areas may have been affected by the rotational stress from σ_2 NNE−SSW and σ_3 NEE–SWW during the development of the Zhaoping detachment fault, resulting in more steep fractures [26]. We tentatively speculate that the anomalous Ag enrichment in the No. 1 orebody of the Dayingezhuang deposit is controlled mainly by the coupled deformation of the Zhaoping and Dayingezhuang faults.

In any case, the flow pathway of deeply sourced ore-forming fluids in the Dayingezhuang deposit was likely variable. The early auriferous fluids that formed the major Au mineralization flowed along the NNE-dipping Zhaoping fault, as suggested in Ref. [7], whereas the later Ag-rich auriferous fluids primarily ascended from distal fractures and/or south oriented conduits. Future exploration should focus on the distal fractures and joints in the south segment of the Dayingezhuang district to search for the vein-style Au(-Ag) mineralization.

6 Conclusions

(1) The Ag mineralization of the Dayingezhuang deposit is primarily associated with the precipitation of Ag-bearing sulfosalts and galena formed as a result of decreasing temperature during the quartz-polymetallic stage. Silver incorporation into galena was dominated by the substitution reaction of $Ag^+ + Bi^{3+} \leftrightarrow 2Pb^{2+}$.

(2) New isotope results suggest that Pb and Ag at the Dayingezhuang deposit were likely transported from metasomatized subcontinental lithospheric mantle and/or modified lower crust. Deep-seated hydrothermal fluids were likely driven by heat from the upwelling asthenosphere during lithospheric thinning.

(3) The Ag enrichment in the No. 1 orebody, particularly for the distal vein-style ore, is a late overprinting ore-forming event that was dominantly controlled by late fluid flow processes driven by shallow brittle structures.

Acknowledgments

The paper greatly benefitted from critical reviews by two anomalous reviewers. We thank Dr. Pete Hollings, Dr. Christopher J. M. Lawley, Prof. Richard Bayless and Prof. Jeffrey M. Dick for their constructive comments on this paper. The first author is grateful for the financial support for studying at Lakehead University by the CSU Special Scholarship for Study Abroad from Central South University. This work is supported by the National Natural Science Foundation of China (Nos. 42030809, 41772349, 41972309, 42072325), and the National Key R&D Program of China (No. 2017YFC0601503).

References

[1] GOLDFARB R, BAKER T, DUBÉ B, GROVES D I, HART C J, GOSSELIN P. Distribution, character and genesis of gold deposits in metamorphic terranes [J]. Economic Geology, 2005, 100: 407−450.

[2] GROVES D I, GOLDFARB R J, GEBRE-MARIAM M, HAGEMANN S, ROBERT F. Orogenic gold deposits: A proposed classification in the context of their crustal distribution and relationship to other gold deposit types [J]. Ore Geology Reviews, 1998, 13: 7−27.

[3] DENG J, YANG L Q, GROVES D I, ZHANG L, QIU K F, WANG Q F. An integrated mineral system model for the gold deposits of the giant Jiaodong province, eastern China [J]. Earth—Science Reviews, 2020, 208: 103274.

[4] GOLDFARB R J, SANTOSH M. The dilemma of the Jiaodong gold deposits: Are they unique? [J]. Geoscience Frontiers, 2014, 5: 139−153.

[5] YANG L Q, DENG J, GOLDFARB R J, ZHANG J, GAO B F, WANG Z L. $^{40}Ar/^{39}Ar$ geochronological constraints on the formation of the Dayingezhuang gold deposit: New implications for timing and duration of hydrothermal activity in the Jiaodong gold province, China [J]. Gondwana Research, 2014, 25: 1469−1483.

[6] SONG M, LI S, SANTOSH M, ZHAO S, YU S, YI P, CUI S, LV G, XU J, SONG Y, ZHOU M. Types, characteristics and metallogenesis of gold deposits in the Jiaodong Peninsula, Eastern North China Craton [J]. Ore Geology Reviews, 2015, 65: 612−625.

[7] MAO X, REN J, LIU Z, CHEN J, TANG L, DENG H, BAYLESS R C, YANG B, WANG M, LIU C. Three-dimensional prospectivity modeling of the Jiaojia-type gold deposit, Jiaodong Peninsula, Eastern China: A case study of the Dayingezhuang deposit [J]. Journal of Geochemical Exploration, 2019, 203: 27−44.

[8] ZHANG L, WEINBERG R F, YANG L Q, GROVES D I, SAI S X, MATCHAN E, PHILLIPS D, KOHN B P, MIGGINS D P, LIU Y. Mesozoic orogenic gold mineralization in the Jiaodong Peninsula, China: A focused event at 120±2 Ma during cooling of pregold granite intrusions [J]. Economic Geology, 2020, 115: 415−441.

[9] LIU Z, MAO X, JEDEMANN A, BAYLESS R C, DENG H, CHEN J, XIAO K. Evolution of pyrite compositions at the Sizhuang gold deposit, Jiaodong Peninsula, Eastern China: Implications for the genesis of Jiaodong-type orogenic gold mineralization [J]. Minerals, 2021, 11: 344.

[10] YUAN Z Z, LI Z K, ZHAO X F, SUN H S, QIU H N, LI J W. New constraints on the genesis of the giant Dayingezhuang gold (silver) deposit in the Jiaodong district, North China Craton [J]. Ore Geology Reviews, 2019, 112: 103038.

[11] TOMKINS A G, GRUNDY C. Upper temperature limits of orogenic gold deposit formation: Constraints from the granulite-hosted Griffin's Find deposit, Yilgarn craton [J]. Economic Geology, 2009, 104: 669−685.

[12] PHILLIPS G N, POWELL R. Formation of gold deposits: A metamorphic devolatilization model [J]. Journal of Metamorphic Geology, 2010, 28: 689−718.

[13] GOLDFARB R J, GROVES D I. Orogenic gold: Common or evolving fluid and metal sources through time [J]. Lithos, 2015, 233: 2−26.

[14] YANG L Q, DENG J, WANG Z L, GUO L N, LI R H, GROVES D I, DANYUSHEVSKY L V, ZHANG C, ZHENG X L, ZHAO H. Relationships between gold and pyrite at the Xincheng gold deposit, Jiaodong Peninsula, China: Implications for gold source and deposition in a brittle epizonal environment [J]. Economic Geology, 2016, 111: 105−126.

[15] YANG L, DENG J, GUO C, ZHANG J, JIANG S, GAO B, GONG Q, WANG Q. Ore-forming fluid characteristics of the Dayingezhuang gold deposit, Jiaodong gold Province, China [J]. Resource Geology, 2009, 59: 181−193.

[16] LI Z, ZHANG R, ZHOU C, QIN W, QIN D. Ore-controlling structure system of Dayin'gezhuang gold deposit in Jiaodong region [J]. Metal Mine, 2010, 405: 86−90. (in Chinese)

[17] SACK R O, GOODELL P C. Retrograde reactions involving galena and Ag-sulphosalts in a zoned ore deposit, Julcani, Peru [J]. Mineralogical Magazine, 2002, 66: 1043−1062.

[18] STAUDE S, DORN A, PFAFF K, MARKL G. Assemblages of Ag−Bi sulfosalts and conditions of their formation: The type locality of schapbachite ($Ag_{0.4}Pb_{0.2}Bi_{0.4}S$) and neighboring mines in the Schwarzwald ore district, southern Germany [J]. The Canadian Mineralogist, 2010, 48: 441−466.

[19] GEORGE L, COOK N J, CIOBANU C L, WADE B P. Trace and minor elements in galena: A reconnaissance LA-ICP-MS study [J]. American Mineralogist, 2015, 100: 548−569.

[20] COSTAGLIOLA P, DI BENEDETTO F, BENVENUTI M, BERNARDINI G P, CIPRIANI C, LATTANZI P F, ROMANELLI M. Chemical speciation of Ag in galena by EPR spectroscopy [J]. American Mineralogist, 2003, 88: 1345−1350.

[21] ZHANG Y, LIU R Q, SUN W, WANG L, DONG Y H, WANG C T. Electrochemical mechanism and flotation of chalcopyrite and galena in the presence of sodium silicate and sodium sulfite [J]. Transactions of Nonferrous Metals Society of China, 2020, 30: 1091−1101.

[22] ZHANG B. Pyrite-sericite-quartz alteration and gold mineralization mechanism of the Dayingezhuang−Xiadian gold-field, Jiaodong peninsula, China [D]. China University of Geosciences (Beijing), 2018. (in Chinese)

[23] TOSDAL R M, WOODEN J L, BOUSE R M. Pb isotopes, ore deposits, and metallogenic terranes [J]. Reviews in Economic Geology, 1999, 12: 1−28.

[24] DENG J, WANG Q, WAN L, YANG L, GONG Q, ZHAO J, LIU H. Self-similar fractal analysis of gold mineralization of Dayingezhuang disseminated-veinlet deposit in Jiaodong gold province, China [J]. Journal of Geochemical Exploration, 2009, 102: 95−102.

[25] YANG B, ZHOU X, DUAN L, WANG H, SHI Q. Tectonic evolution and ore control effect in Dayingezhuang Gold District, Jiaodong Peninsula [J]. Gold, 2020, 41: 35−40. (in Chinese)

[26] DENG J, YANG L Q, LI R H, GROVES D I, SANTOSH M, WANG Z L, SAI S X, WANG S R, LI S. Regional structural control on the distribution of world-class gold deposits: An overview from the Giant Jiaodong Gold Province, China [J].

Geological Journal, 2019, 54: 378−391.

[27] PAN H, ZHANG R, PAN M. Ore-controlling effects of NWW-trending faults in Dayingezhuang gold deposit, Shandong provinve [J]. Gold, 2008, 29: 21−24. (in Chinese)

[28] WEI Y J, QIU K F, GUO L N, LIU X D, TANG L, SHI Q F, GAO X K. Characteristics and evolution of ore-fluids of the Dayingezhuang gold deposit, Jiaodong gold province [J]. Acta Petrologica Sinica, 2020, 36: 1821−1832. (in Chinese)

[29] LAI H, DENG J S, LIU Z L, WEN S M, HUANG L Y. Determination of Fe and Zn contents and distributions in natural sphalerite/marmatite by various analysis methods [J]. Transactions of Nonferrous Metals Society of China, 2020, 30: 1364−1374.

[30] STACEY J S, KRAMERS J D. Approximation of terrestrial lead isotope evolution by a two-stage model [J]. Earth and Planetary Science Letters, 1975, 26: 207−221.

[31] TAN J, WEI J, AUDÉTAT A, PETTKE T. Source of metals in the Guocheng gold deposit, Jiaodong Peninsula, North China Craton: Link to early Cretaceous mafic magmatism originating from Paleoproterozoic metasomatized lithospheric mantle [J]. Ore Geology Reviews, 2012, 48: 70−87.

[32] ZARTMAN R, DOE B. Plumbotectonics—The model [J]. Tectonophysics, 1981, 75: 135−162.

[33] LIU Z, HOLLINGS P, MAO X, LAWLEY C J M, YANG B, TANG L. Metal remobilization from country rocks into the Jiaodong-type orogenic gold systems, Eastern China: New constraints from scheelite and galena isotope results at the Xiadian and Majiayao gold deposits [J]. Ore Geology Reviews, 2021, 134: 104126.

[34] GIULI G, PARIS E, WU Z, de PANFILIS S, PRATESI G, CIPRIANI C. The structural role of Ag in galena (PbS): A XANES study [J]. Physica Scripta, 2005, T115: 387−389.

[35] RENOCK D, BECKER U. A first principles study of coupled substitution in galena [J]. Ore Geology Reviews, 2011, 42: 71−83.

[36] CRAIG J R. Phase relations and mineral assemblages in the Ag−Bi−Pb−S system [J]. Mineralium Deposita, 1967, 1: 278−306.

[37] HODA S N, CHANG L L. Phase relations in the systems PbS−Ag_2S−Sb_2S_3 and PbS−Ag_2S−Bi_2S_3 [J]. American Mineralogist, 1975, 60: 621−633.

[38] HAGEMANN S G, LISITSIN V A, HUSTON D L. Mineral system analysis: Quo vadis [J]. Ore Geology Reviews, 2016, 76: 504−522.

[39] PETTKE T, OBERLI F, HEINRICH C A. The magma and metal source of giant porphyry-type ore deposits, based on lead isotope microanalysis of individual fluid inclusions [J]. Earth and Planetary Science Letters, 2010, 296: 267−277.

[40] LAWLEY C J M, JACKSON S, YANG Z, DAVIS W, EGLINGTON B. Tracing the transition of gold from source to sponge to sink [J]. Economic Geology, 2017, 112: 169−183.

[41] XIONG L, ZHAO X F, WEI J H, JIN X Y, FU L B, LIN Z W. Linking Mesozoic lode gold deposits to metal-fertilized lower continental crust in the North China Craton: Evidence from Pb isotope systematics [J]. Chemical Geology, 2020, 533: 119440.

[42] GIGON J, DELOULE E, MERCADIER J, HUSTON D L, RICHARD A, ANNESLEY I R, WYGRALAK A S, SKIRROW R G, MERNAGH T P, MASTERMAN K J G. Tracing metal sources for the giant McArthur River Zn−Pb deposit (Australia) using lead isotopes [J]. Geology, 2020, 48: 478−482.

[43] CHARLES N, GUMIAUX C, AUGIER R, CHEN Y, ZHU R, LIN W. Metamorphic core complexes vs. synkinematic plutons in continental extension setting: Insights from key structures (Shandong Province, eastern China) [J]. Journal of Asian Earth Sciences, 2011, 40: 261−278.

[44] YANG K F, FAN H R, SANTOSH M, HU F F, WILDE S A, LAN T G, LU L N, LIU Y S. Reactivation of the Archean lower crust: Implications for zircon geochronology, elemental and Sr−Nd−Hf isotopic geochemistry of late Mesozoic granitoids from northwestern Jiaodong Terrane, the North China Craton [J]. Lithos, 2012, 146: 112−127.

[45] TANG H, ZHENG J, YU C, PING X, REN H. Multistage crust–mantle interactions during the destruction of the North China Craton: Age and composition of the Early Cretaceous intrusions in the Jiaodong Peninsula [J]. Lithos, 2014, 190: 52−70.

[46] JAHN B M, LIU D, WAN Y, SONG B, WU J. Archean crustal evolution of the Jiaodong Peninsula, China, as revealed by zircon SHRIMP geochronology, elemental and Nd-isotope geochemistry [J]. American Journal of Science, 2008, 308: 232−269.

[47] STEFáNSSON A, SEWARD T. Experimental determination of the stability and stoichiometry of sulphide complexes of silver (I) in hydrothermal solutions to 400 °C [J]. Geochimica et Cosmochimica Acta, 2003, 67: 1395−1413.

[48] PAL'YANOVA G. Physicochemical modeling of the coupled behavior of gold and silver in hydrothermal processes: Gold fineness, Au/Ag ratios and their possible implications [J]. Chemical Geology, 2008, 255: 399−413.

[49] WILLIAMS-JONES A E, BOWELL R J, MIGDISOV A A. Gold in solution [J]. Elements, 2009, 5: 281−287.

[50] WILKINSON J J, SIMMONS S F, STOFFELL B. How metalliferous brines line Mexican epithermal veins with silver [J]. Scientific Reports, 2013, 3: 1−7.

[51] ESSARRAJ S, BOIRON M C, CATHELINEAU M, TARANTOLA A, LEISEN M, BOULVAIS P, MAACHA L. Basinal brines at the origin of the Imiter Ag−Hg deposit (Anti-Atlas, Morocco): Evidence from LA-ICP-MS data on fluid inclusions, halogen signatures, and stable isotopes (H, C, O) [J]. Economic Geology, 2016, 111: 1753−1781.

[52] YIN Y, ZAJACZ Z. The solubility of silver in magmatic fluids: Implications for silver transfer to the magmatic-hydrothermal ore-forming environment [J]. Geochimica et Cosmochimica Acta, 2018, 238: 235−251.

揭示中国东部胶东半岛大尹格庄金（银）矿床中方铅矿记录的异常银富集作用

刘占坤[1,2]，毛先成[1]，汪凡云[3]，汤 磊[4]，陈光桓[1]，陈 进[1]，邓 浩[1]

1. 中南大学 地球科学与信息物理学院 有色金属成矿预测与地质环境监测教育部重点实验室，长沙 410083；
2. Department of Geology, Lakehead University, Thunder Bay, Ontario P7B 5E1, Canada；
3. 中南大学 出版社，长沙 410083；
4. 招金矿业股份有限公司，烟台 265400

摘 要：通过对方铅矿结构、地球化学和原位铅同位素的研究，探讨大尹格庄金(银)矿床异常银富集的成因。银富集发生晚于金矿化，出现在大尹格庄矿床南部，主要与陡倾裂隙有关的远端脉状矿石中方铅矿及其出溶的富银硫盐矿物(如硫铋银矿)有关。富银方铅矿有最低的放射性成因铅($^{206}Pb/^{204}Pb$ 17.195–17.258 和 $^{208}Pb/^{204}Pb$ 37.706–37.793)，表明变质岩石圈地幔或改造的下地壳为铅和银的源区。这两个镁铁质和超镁铁质源区同样被认为是胶东金矿床中金的源区，暗示深部的金属源区对不均一的银富集作用控制并不显著。由于富银部位同时处于招平和大尹格庄断裂的下盘，因此在 NE–SW 挤压和 NW–SE 伸展背景下，大尹格庄断裂和招平断裂同时活动产生的局部旋转应力最有可能主导不均一的银富集作用。地壳浅部构造活动通过影响后期成矿流体流动进而控制局部金属异常富集。

关键词：方铅矿；铅同位素；银；大尹格庄矿床；胶东半岛

(Edited by Xiang-qun LI)